Joint Experimental−Theoretical Investigation of the Lower Bound States of the NO($X^2\Pi$)-Kr Complex†

Bo Wen and Henning Meyer

Department of Physics and Astronomy, The University of Georgia, Athens, Georgia 30602-2451

Jacek Kłos and Millard H. Alexander*

Department of Chemistry and Biochemistry and Institute for Physical Sciences and Technology, University of Maryland, College Park, Maryland 20742-2021

Received: December 31, 2008; Revised Manuscript Received: February 9, 2009

We describe the first measurement of the near IR spectrum of the NO−Kr van der Waals complex. A variant of IR-REMPI double-resonance spectroscopy is employed in which the IR and UV lasers are scanned simultaneously in such a way that throughout the scan the sum of the two photon energies is kept constant, matching a UV resonance of the system. In the region of the first overtone vibration of the NO monomer, we observe several rotationally resolved bands for the NO−Kr complex. In addition to the origin band located at 3723.046 cm^{-1}, we observe excited as well as hot bands involving the excitation of one or two quanta of *z*-axis rotation. Another band is assigned to the excitation of one quantum of bending vibration. The experimental spectra are compared with results of bound-state calculations for a new set of potential energy surfaces calculated at the spin-restricted coupled cluster level. For the average vibration−rotation energies, there is excellent agreement between the theoretical results based on the coupled states (CS) approximation and the full close-coupling (CC) treatment. Finer details like the electrostatic splitting and the *P*-type doubling of the rotational levels are accounted for only within the CC formalism. The comparison of the CC results with the measured spectra confirms the high quality of the PESs. However, the high resolution of the experiments is sufficient to identify some inaccuracies in the difference between the potential energy surfaces of A' and A'' reflection symmetry.

1. Introduction

Because of the nonadiabatic effects influencing the spectroscopy and dynamics, van der Waals systems containing open shell atoms or molecules have attracted special interest.[1,2] Besides the coupling of the electronic orbital, spin angular momenta, or both with the orbital angular momentum associated with the relative motion of reactants, long-range dispersion forces can enhance reaction by orienting the reactants favorably, especially at energies near a threshold.[3,4] Among the van der Waals systems involving open-shell atoms or molecules, complexes containing the stable radical NO have attracted much interest. In particular, its interaction with various rare gas atoms has been extensively studied both in theory and in experiment.

Over the past decade, significant progress has been made experimentally as well as theoretically in determining the interaction between the molecule NO in its electronic ground state and various rare gas atoms. High-quality ab initio potential energy surfaces (PESs) have been calculated for the interaction with He,[5,6] Ne,[7] and Ar.[8−10] Experimentally, the electronic ground-state interaction with these noble gases has been studied in a great variety of scattering experiments.[11−17] However, the only experimental studies of the ground-state interaction with Kr are the scattering experiments of Thuis et al.[16] and Casavecchia et al.[17]

Spectroscopic information has been limited to the microwave spectra of the complexes of NO with Ar and Ne.[18,19] Also, for these complexes, the intermolecular vibrational levels have been probed with rotational resolution by means of near-IR spectra in the region of the first overtone of NO.[20] For the NO−Ar complex, several low-lying vibrational levels have been probed via MATI spectroscopy without rotational resolution.[21] The spectra agree very well with the predictions of theoretical bound-state calculations for several available ab initio PESs.[7,22]

Electronically excited states van der Waals complexes containing NO have been studied as model systems for the structural and dynamic changes induced by the absorption of light in many-body systems. In particular, the excitation of NO complexes to low-lying Rydberg states and the ensuing structural changes have been investigated in isolated gas-phase clusters[23] and also in the corresponding rare-gas matrices.[24,25] The interaction in Rydberg states is dominated by the interaction of a cationic NO core with the rare-gas atom. The major focus of this research has been complexes of NO with the rare-gas atoms Ne and Ar. The electronic A state of NO−Kr has been measured and analyzed by Wright and coworkers.[26,27] Recently, higher Rydberg states of the NO−Kr system were studied in the gas phase through resonance enhanced multiphoton ionization (REMPI).[28−30]

Although more challenging, several attempts have been made to determine ab initio PESs for the first excited state of these systems.[31,32] The photoexcitation of NO impurities in Kr matrices has been investigated experimentally and theoretically. To simulate the configurational rearrangement of the surrounding of the relaxing impurity molecule, the interactions in both the electronic ground and excited states are required. Recently, Castro-Palacios et al. calculated ab initio PESs of NO−Kr for use in molecular dynamics simulations.[33]

† Part of the "Robert Benny Gerber Festschrift".

* Corresponding author. E-mail: mha@umd.edu.

10.1021/jp811513j CCC: $40.75 © 2009 American Chemical Society
Published on Web 04/23/2009

Very recently, we applied a new variant of IR-REMPI double-resonance spectroscopy to the measurement of the near IR spectrum of the NO−Ar complex.[34] In this double-resonance scheme, the two lasers are scanned simultaneously in such a way that the combined energy of the two photons remains constant. The photon energy sum is chosen to match a UV resonance in the system under investigation. As a result, the 2D frequency problem is reduced to a fixed number of 1D frequency scans. In the case of NO−Ar, we were able to remeasure the previously known bands associated with the intermolecular vibrations with increased resolution and sensitivity.[22] The method allows the detection of weak unknown bands when combined with UV hot-band rather than UV sequence band excitation. For NO−Ar, we detected for the first time the first overtone and combination bands of the intermolecular stretch and bending vibrations. As part of this work, we also detected, for the first time, several hot bands involving levels with one or two quanta of z-axis rotation.

Encouraged by these results, we report in this article the first measurements of the near IR spectrum of NO−Kr in the region of the first vibrational overtone of the NO monomer. Combining the constant photon energy sum scan with UV hot-band detection, we make use of the known (1 + 1) REMPI spectrum of the A state of NO−Kr first reported by Buch et al.[26,27] Depending on the particular photon energy sum, we detected five bands associated with different intermolecular vibrations and quanta of z-axis rotation. The spectra are analyzed with the help of and compared with spectra generated from bound-state calculations for a new set of ab initio PESs. The bound-state energies were determined from full close-coupling (CC) or more approximate coupled-states (CS) calculations.

The article is organized as follows. In the following section, we describe the methodology and the results for the calculation of the PESs. Section 3 is devoted to the bound-state calculations and a comparison of the CC and CS results. In Section 4, we present those details of the experiment relevant to the variant of the IR-REMPI double-resonance scheme employed and the experimental results. Section 5 contains the spectroscopic analysis, including the comparison of experimental and calculated spectra, and a detailed discussion. A conclusion follows.

2. Calculations of the Potential Energy Surface

The intermolecular PESs for the Kr−NO($X^2\Pi$) van der Waals complex were calculated at the spin-restricted coupled cluster level with single, double, and noniterative triple excitations [RCCSD(T)]. We applied the augmented correlation-consistent, triple-ζ basis (aug-cc-pvtz) of Dunning and coworkers for the atoms Kr, N, and O.[35] The basis set was augmented with a set of 3s, 3p, 2d, 2f, and 1g bond functions.[36] Calculations were done with the Molpro suite of ab initio programs.[37] The interaction energy of the complex was calculated by a supermolecular, counterpoise corrected approach where all energies of the dimer and monomers were calculated using a dimer centered basis set.

Ab initio calculations were carried out on a large grid defined by values of the Jacobi coordinate R (the distance between Kr and the center of mass of the NO) ranging from 4.5 to 24 a_0, and θ (the angle between $\vec{R}$ and the NO bond axis) ranging from 0 to 180° in steps of 30°. The NO bond distance was held fixed at its equilibrium value in the $X^2\Pi$ state (1.15077 Å[38]). The angle $\theta = 0$ corresponds to colinear KrNO.

2.1. Features of the Adiabatic and Diabatic Potential Energy Surface. Figures 1 and 2 show contour plots of the electronically adiabatic PESs for the states of A' and A'' reflection symmetry, respectively. The global minimum on the A' PES occurs in T-shaped geometry with $\theta_e = 93°$, $R_e = 7.00a_0$, and $D_e = 146.61$ cm^{-1}. The global minimum on the A'' PES occurs in skewed geometry ($R_e = 7.21a_0$, $\theta_e = 66°$, $D_e = 143.12$ cm^{-1}). There are also additional local minima in the two colinear geometries, where the A' and A'' states are degenerate: for KrNO we find a well depth of 130.35 cm^{-1} located at $R = 8.06a_0$, and for KrON, we find a well depth of 123.45 cm^{-1} at $R = 7.70a_0$.

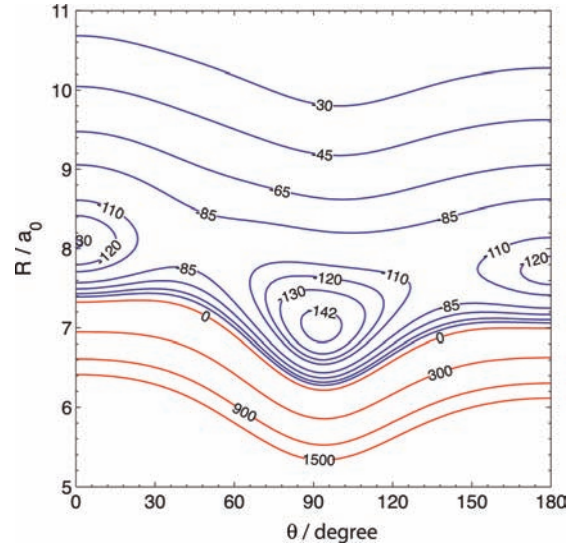

Figure 1. Contour plot of the A' adiabat. Energy in cm^{-1}. $\theta = 0$ corresponds to colinear KrNO.

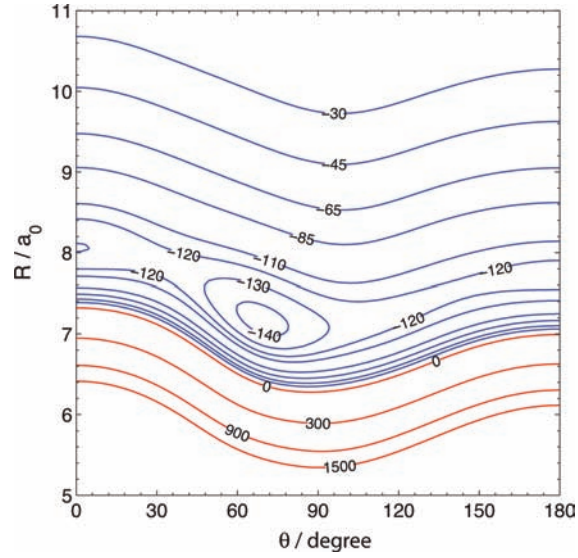

Figure 2. Contour plot of the A'' adiabat. Energy in cm^{-1}. $\theta = 0$ corresponds to colinear KrNO.

The diabatic surfaces V_{sum} and V_{dif} are constructed as the half-sum and the half-difference of the A'' and A' adiabats, respectively[39]

$$V_{sum}(R,\theta) = \frac{1}{2}[V_{A''}(R,\theta) + V_{A'}(R,\theta)] = \sum_{l=0} V_{l0}(R) d^l_{00}(\theta)$$
$$V_{dif}(R,\theta) = \frac{1}{2}[V_{A''}(R,\theta) - V_{A'}(R,\theta)] = \sum_{l=2} V_{l2}(R) d^l_{20}(\theta) \quad (1)$$

The V_{sum} and V_{dif} diabatic PESs are expanded in reduced rotation matrix elements of order of $m = 0$ and 2, respectively.[39]

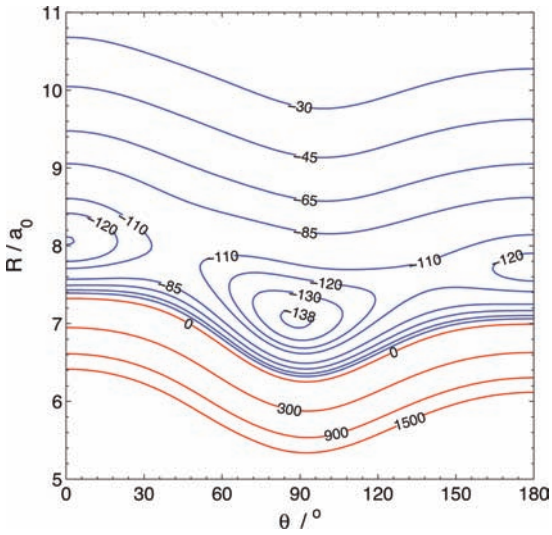

Figure 3. Contour plot of the V_{sum} diabat. Energy in cm^{-1}. $\theta = 0$ corresponds to colinear KrNO.

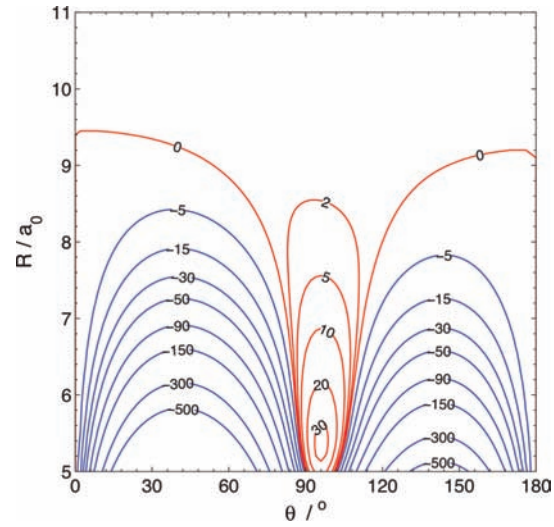

Figure 4. Contour plot of the V_{dif} diabat. Energy in cm^{-1}. $\theta = 0$ corresponds to colinear KrNO.

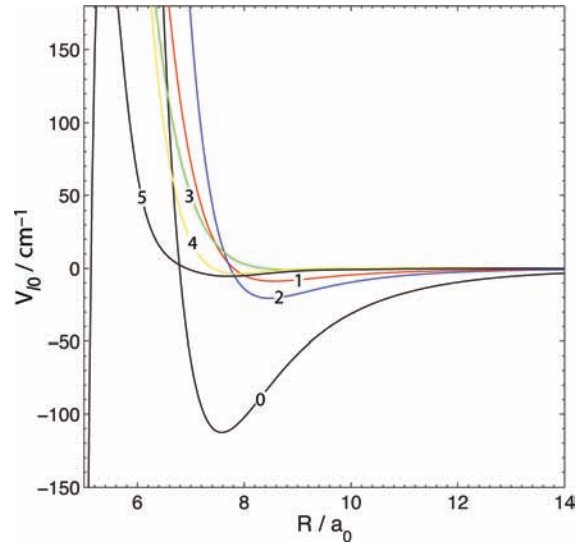

Figure 5. Plot of V_{l0} radial expansion coefficients of the V_{sum} diabat (color online).

In practice, the ab initio points for the A' and A'' PESs were fit separately in a two-step procedure. First, for each value of θ, the R dependence was fit by a variant of the functions introduced by Degli-Esposti and Werner[40]

$$V(R) = G(R)e^{-a_1R-a_2} - T(R)\sum_{n=6}^{9} C_nR^{-n} \quad (2)$$

where

$$G(R) = \sum_{j=0}^{8} g_jR^j \quad (3)$$

and

$$T(R) = 1/2[1 + \tanh(1 + tR)] \quad (4)$$

The parameters a_1, a_2, g_j, and t and the long-range coefficients, C_n, were optimized for each value of θ, separately, by use of a modified Levenberg−Marquardt algorithm for the nonlinear variables and a standard least-squares fit for the linear variables.

Then, for each desired value of R_i and θ_i, eq 2 was used to generate the values of $V_{A'}$ and $V_{A''}$ on the θ grid. From these, the values of V_{sum} and V_{dif} were obtained from eq 1. Finally, the values of the expansion coefficients $V_{l0}(R_i)$ and $V_{l2}(R_i)$ were obtained by solution of sets of linear equations.

Both the V_{sum} diabat and the A' adiabat exhibit near-homonuclear symmetry with respect to $\theta = 90°$. The two-lobed shape of the difference potential (V_{dif}) is typical for NO(X) interacting with a spherical target, similar to He−NO(X).[6] In Figures 5 and 6, we show plots of the radial expansion coefficients of the sum and difference diabats, respectively. Because of the near-homonuclear symmetry, the expansion coefficients with l are even larger than those with l odd.

As mentioned earlier, Castro-Palacios et al.[33] determined an ab initio PES for the A' electronic state of the Kr−NO(X) complex. They used the RCCSD(T) method with an aug-cc-pvtz basis set but without bond functions. The isotropic term V_{00} (eq 1) extracted from our calculations and shown in Figure 5 can be compared with Figure 3 of ref 33. Both isotropic terms are quite similar, with a well depth of 112−115 cm^{-1} occurring at a distance of $\sim 7.6a_0$. In general, for a given value of θ, the minimum on our A' PES occurs at slightly shorter values of R. This is a result of the inclusion of bond functions in our calculations, which are known to improve the description of the attractive (dispersion) contribution to van der Waals interactions.[41] Also, Castro-Palacios et al. do not report calculations of the A'' adiabat, which is crucial to the correct determination of bound states of the NO−Kr complex.

3. Bound-State Calculations

We carried out fully quantum CC and CS calculations of bound states for the set of Kr−NO ($r = r_e$) PESs determined here. In these calculations, the open-shell electronic structure of the NO molecule was taken into account. We employed the HIBRIDON suite of codes.[42]

The radial part of the wave functions in the bound-state calculations is expanded in a replicated Gaussian basis[43] distributed between $R = 4.5$ and 25 a_0. The NO−Kr relative reduced mass was 22.098 amu. The rotational-fine-structure levels of NO($X^2\Pi$) were defined by the rotational constant, B

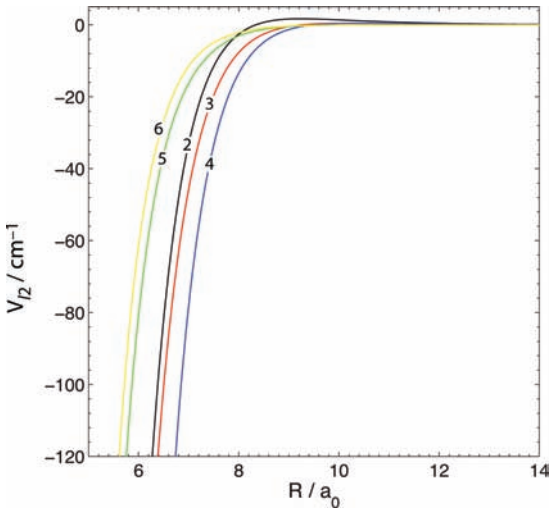

Figure 6. Plot of V_{l2} radial expansion coefficients of the V_{dif} diabat (color online).

= 1.696 cm^{-1}, the spin−orbit constant, A_{so} = 123.139 cm^{-1}, and the Λ-doubling parameters, p = 0.0117 cm^{-1} and q = 0.67 cm^{-1}. The channel basis included all rotational levels of NO up to j_{max} = 12.5, which was sufficient to converge the energies of all bound states for values of the total angular momentum ranging from J = 0.5 to 12.5. In the CS calculations, we retained the same parameters and performed calculations, separately, for each allowed value of the body-frame projection, P, of the total angular momentum $\vec{J}$ ($P = \pm^1/_2, \pm^3/_2, ...$).

In the nonrigid, nearly T-shaped NO−Kr complex, the quantum number P is analogous to the quantum number K of a nearly symmetric top.

To compare quantitatively the experimental spectra with the results of bound-state calculations at different levels of theory, we represent the energy levels by a semiempirical model Hamiltonian that was previously described in detail.[23]

For a nearly T-shaped complex, the main contribution to the rotational energy is a term quadratic in P and thus is independent of the sign of P. This gives rise to a two-fold degeneracy, which is analogous to what is called "asymmetry" doubling in nearly symmetric tops. This doubling is further doubled by the two-fold degeneracy of a Π electronic state in which the energy is independent of the sign of the projection, ω, of the total electronic angular momentum (spin plus orbital) on the NO internuclear axis. Therefore, in the absence of the molecular interaction, each rotational level is four-fold degenerate.

On the basis of work of Green and Lester and Dubernet et al.,[44,45] our model describes the lifting of this four-fold degeneracy as a result of the interaction with the rare-gas atom. The two-fold degeneracy in ω is lifted by V_{sum} to give rise to what we designate as "ω-splitting". In terms of a primitive basis set composed of functions with well-defined (i.e., signed) projections ω and P, the ω splitting removes the degeneracy between basis states for which the products ωP differ in sign. The remaining degeneracy for states with the same product ωP is lifted by V_{dif}, which gives rise to "P-type doubling". Sums and differences of the primitive basis states in P form a basis set of symmetrized functions with well-defined parity, η. Therefore, the levels split by "P-type doubling" can be characterized by different values of η.

For a T-shaped complex, we expect the ω splitting to be more important than the P-type doubling.[46] Depending on the strength of the interaction, the ω splitting can be comparable to or even exceed the spacing of the rotational levels arising from the end-over-end rotation of the complex. In this case, it is more convenient to characterize the groups of energy levels associated with a particular value of ω by an ω-dependent rotational quantum number.[34] Accordingly, we represent the energy levels by the following expression

$$E_{vJP\omega\eta} = E_{vP\omega} + B_\omega J(J+1) + V_\omega\left(J+\frac{1}{2}\right) + \eta\sum_{n=0}^{2}\frac{1}{2}D_{2n}^{\omega}\left(J+\frac{1}{2}\right)^n \quad (5)$$

In a molecular beam environment, NO is cooled primarily to the lower spin−orbit manifold in which $\omega = \pm^1/_2$. Consequently, for simplicity, we will designate the values of ω in the subscripts in eq 5 just by their sign; in other words, $\omega = +$ or $\omega = -$. As discussed above, $\eta = \pm 1$ designates the overall parity of the level. P-type doubling splits these parity levels.

Whereas the experimental spectrum is more easily fitted using eq 5, the subsequent discussion is facilitated by transforming the constants to the ones defined in the model for a weakly perturbed complex[23]

$$E_{vJP\omega\eta} = E_{vP} + B_{vP0}J(J+1) + B_{vP1}\left(J+\frac{1}{2}\right) + \sum_{n=0}^{2}\left(\eta F_{2n} + \frac{\omega}{|\omega|}V_{2n} + \eta\frac{\omega}{|\omega|}C_{2n}\right)\left(J+\frac{1}{2}\right)^n \quad (6)$$

By sorting and comparing the different powers of J, we can easily relate the spectroscopic constants defined here with those that occur in eq 5.[23,34] We find

$$E_{vP} = \frac{1}{2}(E_{vP+} + E_{vP-}), \quad B_{vP0} = \frac{1}{2}(B_+ + B_-),$$
$$B_{vP1} = \frac{1}{2}(V_+ + V_-)$$
$$V_{20} = \frac{1}{2}(E_{vP+} - E_{vP-}) - \frac{1}{8}(B_+ - B_-),$$
$$V_{21} = \frac{1}{2}(V_+ - V_-), V_{22} = \frac{1}{2}(B_+ - B_-),$$
$$F_{2n} = \frac{1}{4}(D_{2n}^{+} + D_{2n}^{-}), \quad \text{and} \quad C_{2n} = \frac{1}{4}(D_{2n}^{+} - D_{2n}^{-}) \quad (7)$$

In the CS approximation, P is a good quantum number. Consequently, we can fit the calculated energy levels directly to eq 5. Although in the CC approach, centrifugal coupling causes the mixing of basis states with different P, this mixing is weak enough that we can, without ambiguity, assign a nominal value of P to each level by comparing the calculated energy of each CC level with the results of the CS calculations.

We have shown that an adiabatic bender model[47,48] provides an excellent approximation for the bound-state energies of many weakly bound complexes of open-shell molecules. Within the CS approximation, for each value of P, diagonalization of the CS Hamiltonian as a function of R yields a set of adiabatic PESs. Solution of a 1D Schrödinger equation gives rise to a set of vibrational levels for the intramolecular (van der Waals) stretch. To a good approximation, n (the cardinal number of the corresponding adiabatic bender potential) and v (the vibrational quantum number within the nth adiabatic bender potential) can

TABLE 1: Spectroscopic Constants (in cm^{-1}) Determined from a Linear Least-Squares Fit of the Calculated CS Energy Levels[a]

ν_b	ν_s	P	$E_{\nu P}$	B_1	B_0	V_{20}	V_{21}
0	0	0.5	−0.024	0.0054	0.0511	0.0259	0.0001
1	0	0.5	14.073	0.0071	0.0442	0.1183	−0.0294
0	1	0.5	19.901	0.0036	0.0467	0.3126	0.0017
2	0	0.5	26.168	0.0041	0.0472	1.3376	0.0008
1	1	0.5	33.932	0.0041	0.0459	1.0733	0.0029
0	2	0.5	40.686	0.0138	0.0432	0.5058	−0.0049
3	0	0.5	43.951	−0.0013	0.0434	0.7784	0.0082
0	0	1.5	3.563	0.0058	0.0512	0.0588	−0.0002
1	0	1.5	21.873	0.0080	0.0470	0.2937	−0.0015
0	1	1.5	27.950	0.0065	0.0475	0.6511	−0.0001
2	0	1.5	36.980	0.0028	0.0463	1.1609	0.0018
1	1	1.5	43.853	0.0078	0.0455	0.9944	0.0021
0	2	1.5	50.204	0.0073	0.0444	0.6848	−0.0003
0	0	2.5	10.647	0.0066	0.0513	0.0706	−0.0003
1	0	2.5	31.593	0.0076	0.0480	0.5106	−0.0010
0	1	2.5	37.166	0.0074	0.0482	0.8843	0.0001
2	0	2.5	50.612	0.0058	0.0464	1.1730	0.0004

[a] Energy levels were fit to the expression given in eq 5. Subsequently, the resulting set of constants was converted to those defined in eq 6 using eq 7.

TABLE 2: Spectroscopic Constants (in cm^{-1}) Determined in a Linear Least-Squares Fit of the Calculated CC Energy Levels[a]

ν_b	ν_s	P	$E_{\nu P}$	B_1	B_0	V_{20}	V_{21}	C_{20}	C_{21}
0	0	0.5	0.015	0.0002	0.0508	0.0088	0.0269	0.0172	0.0005
1	0	0.5	14.113	0.0007	0.0445	0.0622	0.0213	−0.0152	−0.0030
0	1	0.5	19.941	−0.0025	0.0441	0.3222	−0.0083	−0.0499	−0.0297
2	0	0.5	26.167	0.0367	0.0449	1.3014	0.0363	−0.0015	−0.0069
1	1	0.5	33.967	0.0003	0.0467	1.0788	0.0004	0.0003	0.0018
0	2	0.5	40.742	0.0001	0.0438	0.4952	0.0020	−0.0231	−0.0259
3	0	0.5	44.003	−0.0278	0.0488	0.7627	0.0327	−0.0046	−0.0051
0	0	1.5	3.605	0.0003	0.0509	0.0579	0.0002	0.0011	−0.0004
1	0	1.5	21.671	0.1477	0.0315	0.5259	−0.1454	−0.0046	0.0031
0	1	1.5	28.042	−0.0397	0.0469	0.6083	0.0396	−0.0034	0.0021
2	0	1.5	37.005	0.0014	0.0461	1.1565	0.0025	−0.0010	0.0004
1	1	1.5	43.832	0.0542	0.0384	1.1216	−0.0693	0.0281	−0.0098
0	2	1.5	50.202	0.0060	0.0444	0.6674	0.0310	−0.0104	0.0042
0	0	2.5	10.697	0.0010	0.0505	0.0685	0.0005	0.0000	0.0000
1	0	2.5	31.629	0.0025	0.0486	0.5103	−0.0005	0.0000	0.0000
0	1	2.5	37.232	−0.0026	0.0463	0.8791	0.0001	0.0000	0.0000
2	0	2.5	50.652	−0.0042	0.0459	1.1574	0.0043	−0.0008	0.0003

[a] Energy levels were fit to the expression given in eq 5. Subsequently, the resulting set of constants was converted to those defined in eq 6 using eq 7.

be identified with the intramolecular bending ν_b and stretching ν_s quantum numbers of the complex.[34]

The results of the least-squares fits to the calculated CS and CC energies are listed in Tables 1 and 2.

The CS and CC vibrational energies for the individual bend−stretch levels ($E_{\nu P}$) agree extremely well. The average rotational constants, B_0, also agree to within 2%, although a larger discrepancy characterizes the levels with energies near 21 and 44 cm^{-1}. Most likely, this is the effect of a perturbation not included in the CS approximation. Similar agreement characterizes the J-independent contribution to the ω splitting V_{20}, except for the two levels mentioned above.

States corresponding to different values of P are coupled by the centrifugal term in the operator for the kinetic energy of the complex. The magnitude of this effect is manifested in the C_{2n} constants. Consequently, these coefficients vanish in a fit to the CS results because Coriolis coupling is neglected within the centrifugal decoupling approximation that underlies the CS method. In the framework of perturbation theory, the P-type doubling involves the Coriolis operator, V_{dif}, and the spin-uncoupling operator.[44,46] For states with $|P| = 0.5$ and $|\omega| = 0.5$, the Coriolis operator enters linearly to lowest order. Consequently, the J dependence of the P-type doubling is linear.

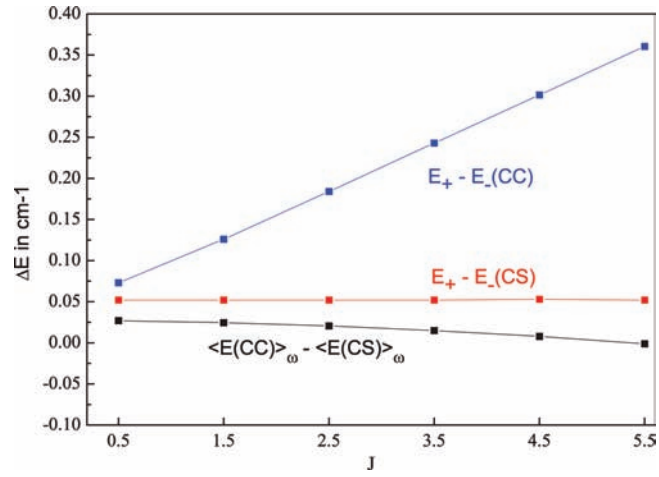

Figure 7. J dependence of the ω splitting $\Delta E(J) = E_{\nu JP(\omega=+)} - E_{\nu JP(\omega=-)}$ for the ground vibrational level ($\nu_b = \nu_s = 0$, $P = 0.5$) of the NO−Kr complex as calculated within the CC (blue) and CS (red) formalism. The black curve represents the deviation of the CS prediction for the ω-averaged energy as a function of J from the corresponding CC result.

Similarly, at the same level of perturbation theory, the odd terms in the expansion of V_{sum}, in particular, $V_{10}(R)$ (Figure 5), will give rise to a linear J dependence for the ω splitting,[23] as manifested in the V_{21} and C_{21} coefficients in eq 6. However, in the CS approximation, the ω splitting is predicted to be nearly independent of J. Therefore, in comparison with the fit to the CC energies, the fit to the results of the CS calculation significantly underestimates the values of V_{21} that are related to the magnitude of the J-dependent contribution to the ω splitting. In Figure 7, we compare the ω splitting as a function of J for the ground vibrational level of NO−Kr ($\nu_b = \nu_s = 0$, $P = 0.5$) from the CC and CS calculations. For the CC curve, we plot the difference between the parity-averaged ω components $E_{\nu JP(\omega=+)}$ and $E_{\nu P(\omega=-)}$, where $E_{\nu P\omega} = 0.5[E_{\nu P\omega(\eta=+1)} + E_{\nu P\omega(\eta=-1)}]$. For the CS calculations, the energies are independent of the sign of P. We also observe, as shown by the black curve in Figure 7, that the average of the energies of the two ω components agrees extremely well for the two types of calculation.

In eq 7, we see that the term V_{21} is related to the difference in the constants V_+ and V_- of eq 5. Because within the CS approximation V_{21} is very small for most vibrational levels, we expect V_+ and V_- to be similar in magnitude and to have the same sign. This, in turn, implies a nonvanishing constant B_1. For most levels, when compared with the fit to the CC energies, the constant B_1 from the fit to the CS energies is too large. (Although, as discussed above, the constant V_{21} is too small.)

In conclusion, we find that whereas the overall vibrational energy is well predicted by the results of the CS calculation, the finer details of the rotational structure require the inclusion of the Coriolis coupling. As will be seen below, the resolution in our experiments is sufficient to require, for their interpretation, a full close-coupled quantum simulation.

4. Experimental Section

4.1. Details of the Experiment. Our different approaches to the IR-UV double-resonance spectroscopy have been previ-

ously described in detail.[22,49] To extend the capabilities and increase the sensitivity of the experiment, we adopted a series of changes that have recently been detailed.[34,50] In brief, the experiments are performed in a differentially pumped molecular beam scattering apparatus.[51,52] Molecular beam pulses with a half-width of about 60−80 μs are generated with a home-built piezoelectric molecular beam valve at a repetition rate of 10 Hz. For the experiments reported in this article, we expanded gas mixtures containing either 2% NO and 5% Kr in Ar or 6% NO and 10% Kr in Ar at backing pressures of 1.5 bar. The pulses enter through a skimmer from the source chamber into the detector chamber. Here they are intersected by the focused IR (500 mm focal length lens) and UV (300 mm focal length lens) lasers in the center of an electrode setup.

When used in the mass spectrometer mode, it consists of an acceleration region and a field-free region, followed by a pair of electrostatic mirrors that deflect the ions off the molecular beam axis toward a microchannel plate (MCP) detector. The time-dependent output of the detector is amplified and recorded with a digital storage oscilloscope (DSO) (Tektronix TDS4000). We recorded IR spectra by averaging waveforms with the DSO for 16 laser shots while scanning the IR laser at a speed of 0.0001 nm/s. The averaged waveforms are transferred to and analyzed by a master PC that controls the experiment.

UV radiation of around 225 nm is generated by frequency doubling the output of a dye laser (LAS LDL205) in a BBO crystal. The dye laser is pumped by the third harmonic of a Nd/YAG laser (Spectra Physics GCR170-10) and operated on the dye Coumarin 460. For hot-band detection of NO−Kr complexes, 400−500 μJ of UV light of around 245 nm is produced by sum frequency generation in the same BBO crystal from the dye laser output and the residual second harmonic radiation from the Nd/YAG laser. The sum frequency light is characterized by a line width of about 2.5 cm^{-1}.

IR radiation near 2.7 μm with an effective line width of about 0.025 cm^{-1} is generated with an OPO laser system (Continuum Mirage 3000). Although in the actual experiment, the signal and idler output are not separated, we typically produce around 3 mJ of radiation at the idler frequency. As in our previous experiments, we monitor the fringes of an etalon (free spectral range (FSR) = 0.200918 cm^{-1}, finesse 12) and the photo acoustic cell spectrum of NO during a scan of the IR laser. Whereas the etalon fringes establish the relative frequency scale for the scan, the first overtone spectrum of NO provides the absolute frequency calibration.[53] Using a pair of digital delay generators, the IR laser is fired 30 ns before the UV probe laser. The UV laser beam crosses the molecular beam at a right angle while the IR laser beam makes an angle of 12° with the UV beam. Both lasers are polarized in the plane formed by the two laser beams and the molecular beam.

4.2. Experimental Results. Two spectroscopic schemes are employed in this work to detect electronic ground-state NO−Kr complexes with $\nu_{NO} = 0$ and $\nu_{NO} = 2$. To verify and to optimize the molecular beam source performance, we use 1 + 1 REMPI to detect NO($\nu_{NO} = 0$)−Kr in the region of the X−A transition of the NO monomer: NO $X^2\Pi$ ($\nu'' = 0$) → NO A $^2\Sigma$ ($\nu' = 0$). Vibrationally excited NO($\nu_{NO} = 2$)−Kr complexes are detected in the region of the associated hot-band transition of the monomer: NO $X^2\Pi$ ($\nu'' = 2$) → NO A $^2\Sigma$ ($\nu' = 0$). We use narrow bandwidth SHG radiation near 225 nm for the former but relatively broadband sum frequency UV around 245 nm for the latter.[54]

As shown in Figure 8, in the case of A-state detection, NO−Kr cluster signals attributed to the parent cluster are

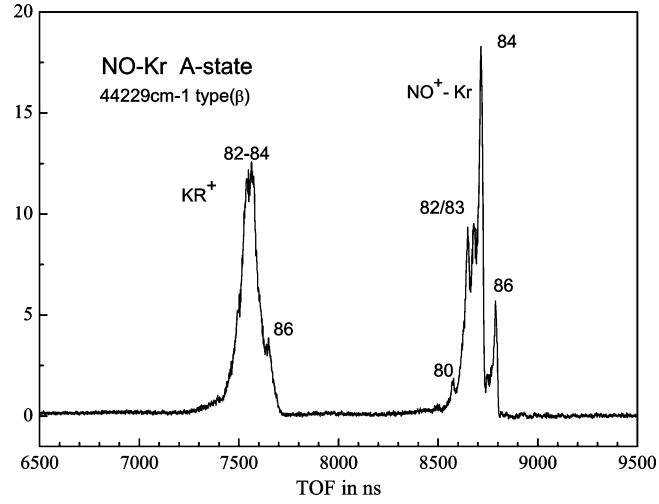

Figure 8. TOF spectrum recorded at 44 229 cm^{-1} (type(β)). Peaks are labeled with the masses of the different isotopes of Kr.

detected in both the NO−Kr^+ and the Kr^+ mass channels. Different isotope peaks are resolved only for the parent ion NO−Kr^+. Although we operate the electrode setup in a mass spectrometer rather than a velocity dispersion mode, the setup is still somewhat sensitive to the velocities of the neutrals before ionization. Because of the energy release during the fragmentation process, the fragments Kr^+ will be characterized by a distribution of kinetic energies, which causes the different isotope peaks to overlap. However, we expect the velocity distribution for the parent ions to be solely determined by the velocity spread of the neutral clusters in the beam. Being able to resolve the different isotopes for NO−Kr^+ thus provides strong evidence of these ions directly forming from the neutral parent complex, NO−Kr. We recorded frequency spectra by monitoring the integral over all isotopes of the Kr and the NO−Kr ion mass peaks.

When an IR-UV double-resonance scheme is used to measure IR spectra of molecules or clusters, a problem arises when the UV detection step does not match a UV resonance in the system under investigation. As we described in ref 34, these problems can be avoided by scanning the IR and UV lasers simultaneously in opposite directions to keep the sum of the two photon energies constant throughout the scan. By choosing the photon energy sum to match a known UV resonance in the system, the 2D frequency problem is reduced to a fixed number of 1D constant photon energy scans.

The structured spectrum of the NO−Kr complex in the region of the monomer X−A transition was first reported by Bush et al.[26,27] In Figure 9, we compare the 1 + 1 REMPI spectra recorded in the Kr^+ and the NO−Kr^+ ion channels with the double-resonance spectrum for the hot-band region. The small negative structures near 44 200 cm^{-1} at 44 240 and 44 275 cm^{-1} are due to baseline shifts caused by strong signals from the NO monomer and the NO−Ar complex, respectively. The hot-band spectrum was recorded in the NO−Kr ion mass channel with the IR frequency fixed to the Q branch of the origin band of NO−Kr at 3723.0463 cm^{-1}. To align the different peaks in both types of spectra, we shifted the double-resonance spectrum up in frequency by the energy of the IR pump photon. Apart from the increased line width of the different peaks, all major peaks are reproduced in the double-resonance spectrum with similar intensities. Following the convention adopted in ref 34, we designate the major peaks as α through ϕ. Their frequencies define constant photon energy sums of type (α) through type (ϕ).

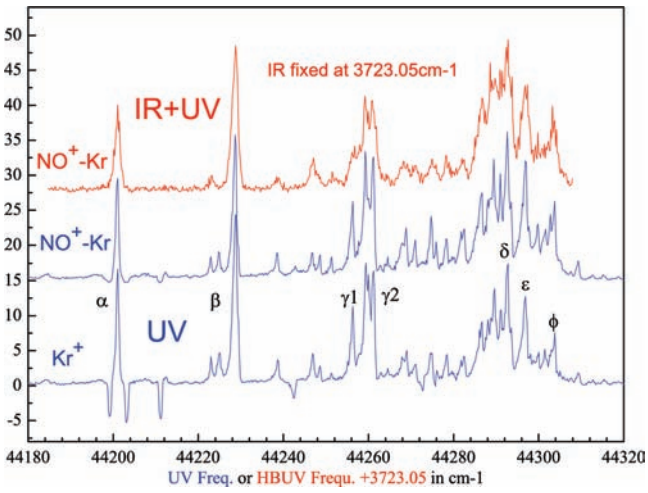

Figure 9. 1 + 1 REMPI spectrum of NO−Kr recorded in the ion channels for Kr^+ (blue) and NO^+ −Kr (blue). The red curve represents an IR-REMPI double-resonance spectrum with the IR frequency fixed to 3723.0463 cm^{-1}. During this scan, the frequency of the UV for exciting the hot-band transition is scanned. To align the peaks in the different spectra, we shifted the hot-band spectrum up in frequency by the energy of the IR photon.

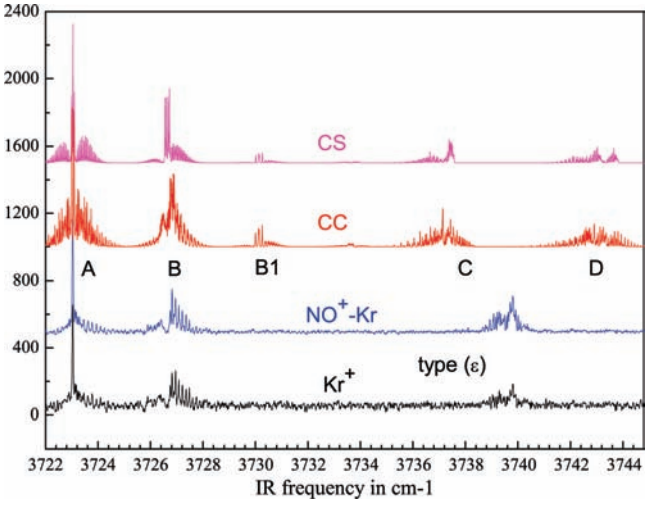

Figure 10. Constant photon energy sum scan of type (ε). The signal was monitored on the indicated ion masses. The top two traces represent simulated spectra based on the results of the CS and the CC calculations assuming a temperature of 2 K.

As an example, we show in Figure 10 the double-resonance spectra of type (ε) recorded in the Kr and NO−Kr mass channels. Apart from the slightly poorer signal-to-noise ratio for the spectrum recorded in the Kr channel, the two experimental spectra are identical.

The top two traces in this Figure represent spectra generated from the results of the bound-state calculations using the CS and the CC approximation. The theoretical spectra show four bands, labeled A through D. In addition, we included in the theoretical spectra the hot-band B1. Band A represents the origin of the near-IR spectrum of NO−Kr in the region of the first overtone spectrum of NO. Bands C and D are due to excitation of one quantum of bending and stretch vibration, respectively. Band B represents the excitation of one quantum of *z*-axis rotation in NO−Kr. Apart from the rotational fine structure, the energies of the NO−Kr complex are labeled by the vibrational quantum number of NO, ν_{NO}, the NO−Kr bending and stretch vibrational quantum numbers, ν_b and ν_s, and the quantum number, *P*, describing the *z*-axis rotation, namely, (ν_{NO}, ν_s, ν_b, *P*). The hot-band B1 involves transitions of the type: (0, 0, 0, 1.5) → (2, 0, 0, 2.5) Note that a constant photon energy sum as defined by the type (α) and so on defines resonances involving the ground-state level (0, 0, 0, 0.5) of NO−Kr. Because hot bands involve an excited level, they are detected only in those scans for which there is a fortuitous coincidence. This is indeed the case for the spectrum recorded as type (δ). (See below.)

The experimental spectrum is dominated by band A centered at 3723.046 cm^{-1} and two weaker bands, B and C, located at 3726.644 and 3739.571 cm^{-1}, respectively. Band A is dominated by a strong Q branch, whereas weak rotational R and P branches are observed at higher and lower frequencies, respectively. It is assigned to the origin band of the first NO overtone transition in NO−Kr. Band B agrees well with the second band predicted by theory and is therefore assigned to the excitation of one quantum of *z*-axis rotation. As discussed above, the associated hot-band B1 is not observed in this spectrum. The third band observed experimentally exhibits rotational structures similar to the calculated band C, which is assigned to the excitation of one quantum of bending vibration. Compared with the predicted one, it is shifted roughly 2.4 cm^{-1} toward higher energy. Despite extensive searches (up to 3750 cm^{-1}), we have not been able to detect band D, which represents the excitation of the intermolecular stretch vibration. An explanation for the absence of this band in the experimental spectra is more likely to be found in an unfavorable Franck−Condon factor for the IR transition rather than for the UV transition. This is especially true because we probed the IR spectrum with various types of photon energy sums accessing the ground level of the electronically excited state as well as states lying close to the A-state dissociation limit. Similarly, vibrational predissociation is improbable because of the large amount of excess energy necessarily channeled into NO rotation and, importantly, into fragment translation.

Compared with the NO−Ar system, the A state of NO−Kr offers many more bound levels that can be used as the final state for a constant photon energy sum scan. In this work, we recorded spectra of type (α), type (β), type (δ), and type (ε) corresponding to photon energy sums of 44 201.2, 44 228.8, 44 292.7, and 44 297.0 cm^{-1}, respectively. Except for the spectrum recorded as type (α), all spectra show bands A, B, and C with similar intensities and almost identical rotational fine structure. Figure 11 displays the different types for bands A and B. Note that the signal-to-noise ratio for the spectra recorded as types (α) and (ε) is not as good because a more diluted gas mixture was used for the molecular beam expansion.

5. Spectroscopic Analysis and Discussion

As described in ref 23, we generate theoretical spectra by neglecting any dependence of the bound-state energy on the NO vibration. Therefore, we assume that the sets of PESs for NO(ν_{NO} = 0)−Kr and for NO(ν_{NO} = 2)−Kr are identical. This assumption is supported by the very small red shift of the NO−Kr spectrum with respect to the origin of the NO monomer but also by the small variation in the fitted constants of band B and the constants derived for the corresponding hot-band HB. (See below.)

With these limitations in mind, we generate a theoretical near-IR spectrum by shifting the energy differences between the levels found in the calculations by the frequency corresponding to the experimentally observed center of the NO−Kr origin band: 3723.046 cm^{-1}. As described in ref 23, we work within

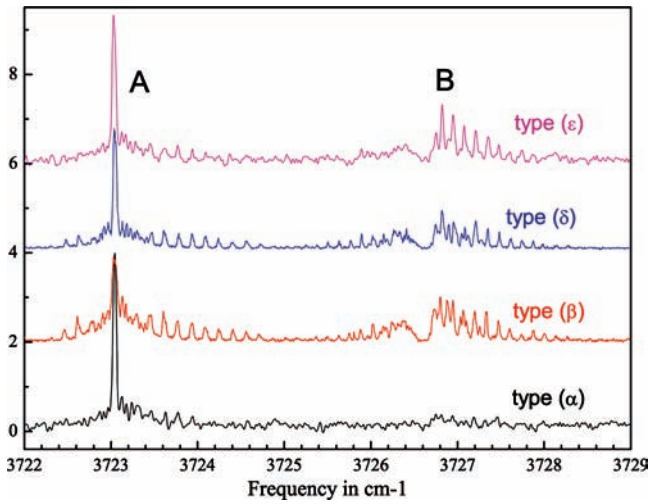

Figure 11. Comparison of constant photon energy sum scans of types (α), (β), (δ), and (ε) through the region of bands A and B.

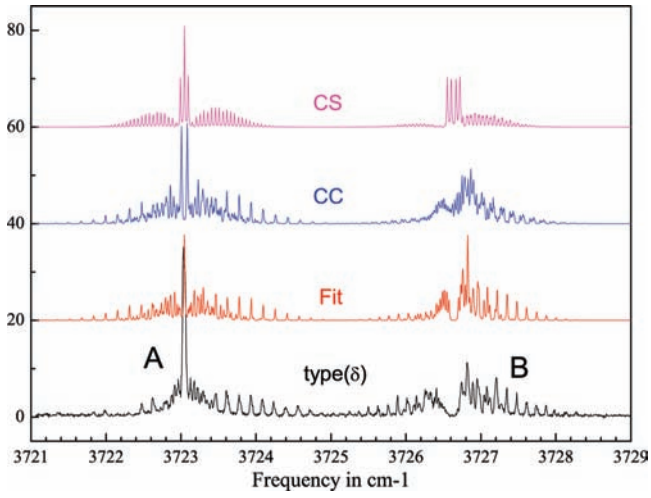

Figure 12. Comparison of the spectra generated from the CS and the CC data with the experimental spectrum of type (δ) and its fit: bands A and B.

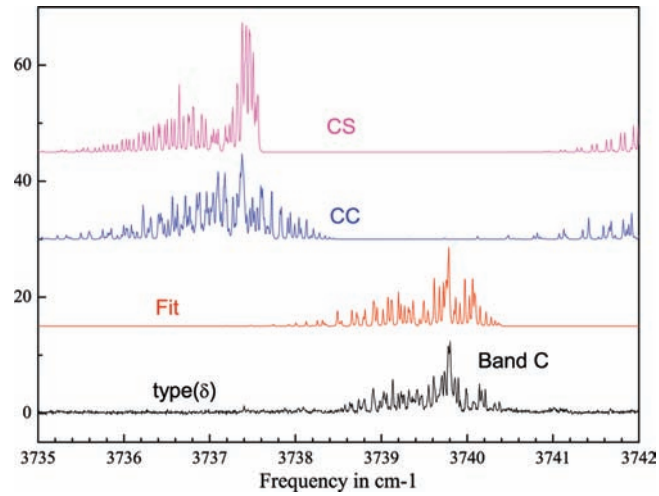

Figure 13. Comparison of the spectra generated from the CS and the CC data with the experimental spectrum of type (δ) and its fit: band C.

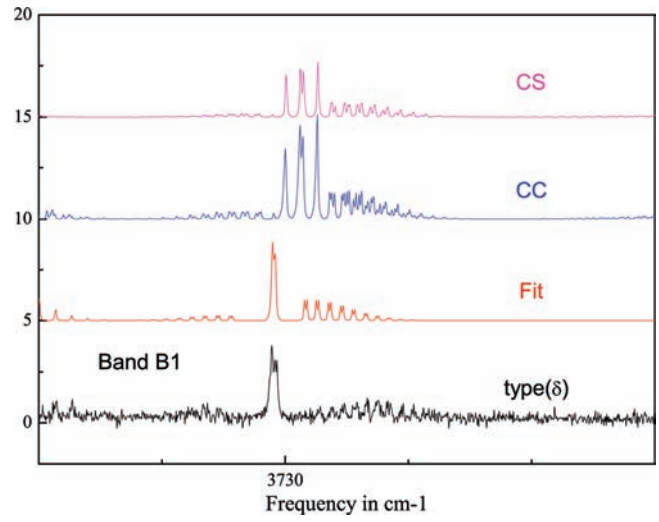

Figure 14. Comparison of the spectra generated from the CS and the CC data with the experimental spectrum of type (δ) and its fit: hot-band B1.

the adiabatic bender approximation[47,48] to calculate an approximate rotational line strength factor. Both parallel and perpendicular components of the transition moment vector are included with their ratio kept as an adjustable parameter. Finally, the overall intensity of a band is adjusted empirically through a Franck−Condon factor assuming a Boltzmann distribution with a temperature of 2 K.

Using the parameters from the fits to the results of the CS and CC calculation (Tables 1 and 2), we generate spectra including vibrational bands with up to 50 cm^{-1} in excitation energy. The resulting spectra are displayed in the top part of Figure 10. We also show the calculated spectrum for the hot-band B1 involving transitions from the ground-state levels with $P = 1.5$ to excited-state levels with $P = 2.5$. The comparison of the rotational fine structure with the experimental spectra is shown in Figures 12−15. In these Figures, we include a spectrum based on a set of spectroscopic constants fitted to match the experimental one. The results of this fit are listed in Table 3. In fitting, we use only as many constants as are necessary to reproduce the experimental spectra accurately. It turns out that a very good match can be achieved by applying the constraints $D^{\omega}_{2n} = 0$ and $V_+ = -V_-$, that is, $B_1 = 0$. Consequently, it is the ω-splitting terms both constant and linear in J that are responsible for the rotational fine structure. At the resolution of our experiment, the P-type doubling is not apparent except for a possible broadening of the Q branch of band A.

Comparing the results of the fit with the predictions of the CC calculation, we find good agreement for the vibrational energy of band B, whereas band C is predicted 2.4 cm^{-1} too low in energy. However, the rotational constants B_1 and B_0 agree very well. For the ground vibrational level, we observe a similar trend for the ω splitting, whereas the P-type doubling is clearly overestimated in the CC treatment. This difference is most clearly demonstrated in the predicted splitting of the Q branch of band A. In terms of possible ω transitions, we can distinguish ω-preserving and ω-changing transitions. According to eq 5, we find for the Q branch position with $\Delta\omega = 0$

$$\Delta E_{\omega'\omega'\eta'\eta''} = +(\eta' - \eta'')\frac{1}{2}D^{\omega'}_{20} \quad \text{and} \quad \Delta\omega = 0 \qquad (8)$$

Because two ω transitions contribute at the same frequency, we expect the associated spectral feature to be dominant. Its splitting is solely due to P-type doubling.

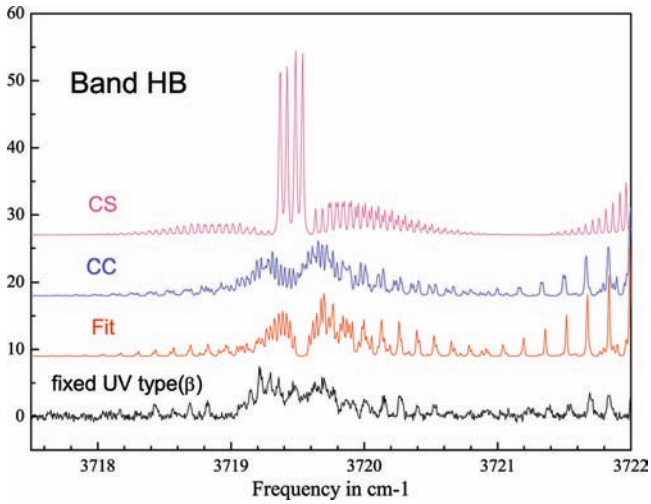

Figure 15. Comparison of the spectra generated from the CS and the CC data with the experimental spectrum of type (δ) and its fit: hot-band HB.

TABLE 3: Spectroscopic Constants (in cm^{-1}) Determined by Fit to the Experimental Spectrum[a]

ν_{NO}	ν_b	ν_s	P	$E_{\nu P}$	B_0	V_{20}	V_{21}
0	0	0	0.5	0.005	0.0505	0.0050	0.0300
0	0	0	1.5	3.520	0.0505	0.0100	0.0000
2	0	0	0.5	0.005	0.0505	0.0050	0.0300
2	0	0	1.5	3.598	0.0506	0.0025	0.0000
2	0	0	2.5	10.390	0.0502	0.0000	0.0000
2	1	0	0.5	16.525	0.0446	0.1750	−0.0300

[a] In the fit, the constants B_1, F_{2n}, and C_{2n} (eq 3) were set to zero.

For ω-changing transitions and assuming symmetric splittings, namely, $E_\omega = -E_{-\omega}$ and similarly for V_ω and D^ω, we find

$$\Delta E_{\omega'(-\omega')\eta'\eta''} = 2E_{\upsilon P\omega'} + 2V_{\omega'}\left(J + \frac{1}{2}\right) + (\eta' + \eta'')D_{20}^{\omega'} \tag{9}$$

Because for a one-photon transition the parity has to change, the last term vanishes; therefore, these lines do not exhibit P-type doubling. As a result, we expect two satellite branches with constant line spacing on each side of the dominant feature discussed above.

For the CS approximation, we find $V_{21} \approx 0$, which causes the two satellite branches to collapse into a single line on each side of the central Q branch. Obviously, the latter cannot be split because of the absence of the P-type doubling. As a result, band A in the CS treatment exhibits three central lines. In the case of the vibrational levels involved in the transitions having different constants V_{20}, we expect a splitting of the central peak. This is the case for bands B and HB for which the Q branch transitions result in four well-separated lines. For the hot-band B1, the central peak is not fully split because the constants V_{20} differ by an amount comparable to the experimental resolution.

The absence of P-type doubling in the results of the CS calculation is also responsible for the overall appearance of the various bands with respect to their rotational fine structure. The lack of splitting results in the absence of the grouping of the lines, which is apparent in both the experimental spectra and those predicted by the results of the CC calculations. The most important residual differences between experiment and the CC calculations is the splitting of the Q branch in band A and band B1. Also, the higher R- and P-branch lines in bands B, B1, and HB are doubled. This doubling is not seen in the experimental spectra.

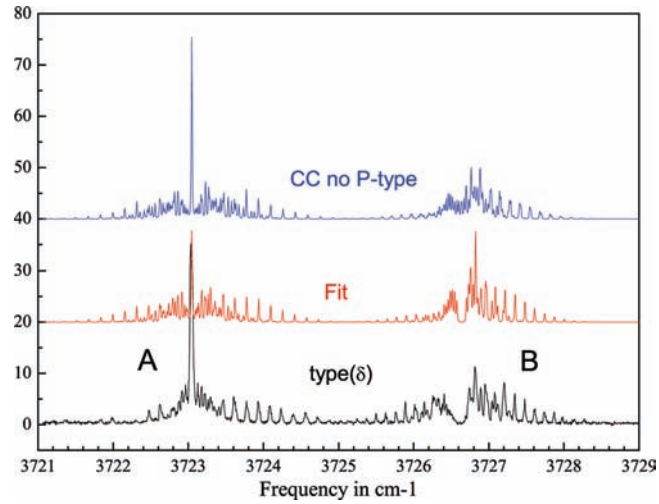

Figure 16. Comparison of the experimental spectrum of type (δ) and its fit with a spectrum generated from the CC data but with the P-type doubling constants, C_{2n}, set to zero (eqs 6 and 7). The CC spectra in this Figure should be compared with those in Figure 12.

To confirm the origin of these splittings, we show in Figure 16 a calculated spectrum based on the fit to the CC energies and then subsequently setting the P-type doubling constants to zero. Comparison of Figures 12 and 16 shows that neglect of the P-type doubling greatly improves the agreement of the predicted spectra with experiment, reducing the magnitude of the splitting in the Q branch and the doubling in the R branch.

In the experiment, we also measured hot bands involving the level (ν_{NO}, ν_s, ν_b, P) = (0, 0, 0, 1.5) in transitions to the excited levels (2, 0, 0, 0.5) and (2, 0, 0, 2.5). The latter, denoted B1, is shown in Figure 14 and the former, denoted HB, is displayed in Figure 15 together with the theoretical and fitted spectra. A careful examination of the fitted spectroscopic constants in Table 3 demonstrates the very small changes due to the change of the NO monomer vibration. For the level with $P = 1.5$, the energy changes by less than 0.1 cm^{-1}, whereas, within the accuracy of the fit, the rotational constants cannot be distinguished. Also, the difference in the ω-splitting constant is very close to the effective experimental resolution. In combination with the small red shift from the origin of the monomer spectrum, we conclude that the NO($\nu = 0$)−Kr and the NO($\nu = 2$)−Kr sets of PESs are very similar.

6. Conclusions

We have used constant photon energy sum scans to measure the rotationally resolved near-IR spectrum of the NO−Kr complex. The origin band of the complex is red-shifted by 0.80 cm^{-1} from the corresponding NO monomer first overtone transition. Two additional bands assigned to the excitation of z-axis rotation and bending vibration were recorded. We also detected two hot bands involving the first excited level for z-axis rotation. The small red shift and the small variation in the spectroscopic constants derived for the excited bands and the hot bands lend support to the assumption that the sets of PESs correlating with Kr + NO($\nu = 0$) and with Kr + NO($\nu = 2$) are very similar.

The spectra are compared with the results of CC and CS bound-state calculations for a new set of ab initio PESs. The comparison is facilitated by representing the theoretical bound-

state energies through a set of spectroscopic constants. In addition to the vibrational and rotational energy, the constants describe the electrostatic ω splitting due to the average potential and the *P*-type doubling caused by the difference potential.

Whereas both theoretical treatments agree very well in the vibrational and average rotational energies, the CS approximation falls short both by missing the *P*-type doubling completely and by not predicting a dependence on *J* of the ω splitting. Consequently, only a comparison of full CC calculations with experiment can provide a complete assessment of the quality of the underlying PESs.

We find excellent agreement for the position and the overall rotational structure of the *P* levels associated with the lowest intramolecular (van der Waals) vibrational level of NO−Kr. The position of the band assigned to the first intramolecular bending vibration is predicted within several wavenumbers. For all of the observed bands, the ω splitting and its *J* dependence are in good agreement with the predictions of our CC calculations. However, these calculations overestimate the magnitude of the *P*-type doubling. Therefore, comparison with experiment confirms the high overall quality of the ab initio PESs, in particular the average (V_{sum}) of the PESs for the states of A' and A'' reflection symmetry. The discrepancies in the prediction of the magnitude of the *P*-type doubling may be due to residual inaccuracies in the difference potential (V_{dif}).

Acknowledgment. We are grateful to the U.S. National Science Foundation for financial support under grant nos. CHE-0097189 (to H.M.) and CHE-0848110 (to M.H.A.).

References and Notes

(1) Carter, C. C.; Lee, H. S.; McCoy, A. B.; Miller, T. A. *J. Mol. Struct.* **2000**, *525*, 1.
(2) Heaven, M. C. *Int. Rev. Phys. Chem.* **2005**, *24*, 375.
(3) Skouteris, D.; Manolopoulos, D. E.; Bian, W.; Lai, L.-H.; Liu, K. *Science* **1999**, *286*, 1713.
(4) Klos, J.; Szczesniak, M. M.; Chalasinski, G. *Int. Rev. Phys. Chem.* **2004**, *23*, 541.
(5) Lee, E. P.; Wright, T. G. *J. Chem. Phys.* **1998**, *109*, 157.
(6) Klos, J.; Chalasinski, G.; Berry, M. T.; Bukowski, R.; Cybulski, S. *J. Chem. Phys.* **2000**, *112*, 2195.
(7) Alexander, M. H.; Soldan, P.; Wright, T. G.; Kim, Y.; Meyer, H.; Dagdigian, P. J.; Lee, E. P. F. *J. Chem. Phys.* **2001**, *114*, 5588.
(8) Alexander, M. H. *J. Chem. Phys.* **1999**, *111*, 7426.
(9) Alexander, M. H. *J. Chem. Phys.* **1999**, *111*, 7435.
(10) Sumiyoshi, Y.; Endo, Y. *J. Chem. Phys.* **2007**, *127*, 184309.
(11) (a) Andresen, P.; Joswig, H.; Pauly, H.; Schinke, R. *J. Chem. Phys.* **1982**, *77*, 2204. (b) Joswig, H.; Andresen, P.; Schinke, R. *J. Int. Biomed. Inf. Data* **1986**, *85*, 1904.
(12) James, P. L.; Sims, I. R.; Smith, I. W. M.; Alexander, M. H.; Yang, M. *J. Chem. Phys.* **1998**, *109*, 3882.
(13) Kim, Y.; Meyer, H.; Alexander, M. H. *J. Chem. Phys.* **2004**, *121*, 1339.
(14) Lorenz, K. T.; Chandler, D. W.; Barr, J. W.; Chen, W.; Barnes, G. L.; Cline, J. I. *Science* **2001**, *293*, 2063.
(15) Kohguchi, H.; Suzuki, T.; Alexander, M. H. *Science* **2001**, *294*, 832.
(16) Thuis, H.; Stolte, S.; Reuss, J.; van den Biesen, J. J. H.; van den Meijdenberg, C. J. N. *Chem. Phys.* **1980**, *52*, 211.
(17) Casavecchia, P.; Lagana, A.; Volpi, G. G. *Chem. Phys. Lett.* **1984**, *112*, 445.
(18) Mills, P. D. A.; Western, C. M.; Howard, B. J. *J. Phys. Chem.* **1986**, *90*, 3331.
(19) Mills, P. D. A.; Western, C. M.; Howard, B. J. *J. Phys. Chem.* **1986**, *90*, 4961.
(20) Kim, Y.; Patton, K.; Fleniken, J.; Meyer, H. *Chem. Phys. Lett.* **2000**, *318*, 522.
(21) Monti, O. L. A.; Cruse, H. A.; Softley, T. P.; Mackenzie, S. R. *Chem. Phys. Lett.* **2000**, *333*, 146.
(22) Kim, Y.; Fleniken, J.; Meyer, H.; Alexander, M. H.; Dagdigian, P. J. *J. Chem. Phys.* **2000**, *113*, 73.
(23) Kim, Y.; Meyer, H. *Int. Rev. Phys. Chem.* **2001**, *20*, 219.
(24) Vigliotti, F.; Bonacina, L.; Chergui, M.; Rojas-Lorenzo, G.; Rubayo-Soneira, J. *Chem. Phys. Lett.* **2002**, *362*, 31.
(25) Apkarian, V. A.; Schwentner, N. *Chem. Rev.* **1999**, *99*, 1481.
(26) Buch, A. M.; Dyke, J. M.; Mack, P.; Smith, D. M.; Wright, T. G. *J. Chem. Phys.* **1996**, *105*, 9804.
(27) Gamblin, S. D.; Daire, S. E.; Lozeille, J.; Wright, T. G. *Chem. Phys. Lett.* **2000**, *325*, 232.
(28) Bergeron, D. E.; Musgrave, A.; Gammon, R. T.; Ayles, V. L.; Silber, J. A. E.; Wright, T. G.; Wen, B.; Meyer, H. *J. Chem. Phys.* **2006**, *124*, 214302.
(29) Wen, B.; Meyer, H.; Ayles, V. L.; Musgrave, A.; Bergeron, D. E.; Silber, J. A. E.; Wright, T. G. *Phys. Chem. Chem. Phys.* **2008**, *10*, 375.
(30) Kłos, J.; Alexander, M. H.; Hernandez-Lamoneda, R.; Wright, T. G. *J. Chem. Phys.* **2008**, *129*, 244303.
(31) Shafizadeh, N.; Brechignac, Ph.; Dyndgaard, M.; Fillion, J. H.; Gauyasq, D.; Levy, B.; Miller, J. C.; Pino, T.; Raoult, M. *J. Chem. Phys.* **1998**, *108*, 9313.
(32) Ayles, V. L.; Plowright, R. J.; Watkins, M. J.; Wright, T. G.; Klos, J.; Alexander, M. H.; Pajon-Suarez, P.; Rubay-Soneira, J.; Hernandez-Lamoneda, R. *Chem. Phys. Lett.* **2007**, *441*, 181.
(33) Castro-Palacios, J. C.; Rubayo-Soneira, J.; Ishii, K.; Yamashita, K. *J. Chem. Phys.* **2007**, *126*, 134315.
(34) Wen, B.; Kim, Y.; Meyer, H.; Klos, J.; Alexander, M. H. *J. Phys. Chem. A* **2008**, *112*, 9483.
(35) Tao, F.-M.; Pan, Y.-K. *J. Chem. Phys.* **1992**, *97*, 4989.
(36) (a) Dunning, T. H., Jr. *J. Chem. Phys.* **1989**, *90*, 1007. (b) Kendall, R. A.; Dunning, T. H., Jr.; Harrison, R. J. *J. Int. Biomed. Inf. Data* **1992**, *96*, 6796.
(37) Werner, H.-J.; Knowles, P. J.; Lindh, R.; Manby, F. R.; Schütz, M.; et al. *Molpro: A Package of Ab Initio Programs*, version 2006.1; University College Cardiff Consultants, Ltd.: Cardiff, U.K., 2006.http://www.molpro.net.
(38) Huber, K. P.; Herzberg, G. *Molecular Spectra and Molecular Structure. IV. Constants of Diatomic Molecules*; Van Nostrand Reinhold: New York, 1979.
(39) (a) Alexander, M. H. *J. Chem. Phys.* **1982**, *76*, 5974. (b) Alexander, M. H. *Chem. Phys.* **1985**, *92*, 337.
(40) Degli-Esposti, A.; Werner, H.-J. *J. Chem. Phys.* **1990**, *93*, 3351.
(41) Burcl, R.; Chałasiński, G.; Bukowski, R.; Szcześniak, M. M. *J. Chem. Phys.* **1990**, *103*, 1498.
(42) Alexander; M. H.; Manolopoulos, D. E.; Werner, H.-J.; Follmeg, B.; Vohralik, P. F.; Lemoine, D.; Corey, G.; Gordon, R.; Johnson, B.; Orlikowski, T.; Berning, A.; Degli-Esposti, A.; Rist, C.; Dagdigian, P.; Pouilly, B.; van der Sanden, G.; Yang, M.; de Weerd, F.; Gregurick, S.; Kłos, J. *Hibridon*; University of Maryland: College Park, MD; a package of programs for the time-independent quantum treatment of inelastic collisions and photodissociation.
(43) Hamilton, I. P.; Light, J. C. *J. Chem. Phys.* **1986**, *84*, 306.
(44) Green, W. H.; Lester, M. I. *J. Chem. Phys.* **1992**, *96*, 2573.
(45) Dubernet, M. L.; Flower, D.; Hutson, J. M. *J. Chem. Phys.* **1991**, *94*, 7602.
(46) Dubernet, M. L.; Tuckey, P. A.; Hutson, J. M. *Chem. Phys. Lett.* **1992**, *193*, 355.
(47) Holmgren, S. L.; Waldman, W.; Klemperer, W. *J. Chem. Phys.* **1977**, *67*, 4414.
(48) Alexander, M. H.; Gregurick, S.; Dagdigian, P. J. *J. Chem. Phys.* **1994**, *101*, 2887.
(49) Kim, Y.; Fleniken, J.; Meyer, H. *J. Chem. Phys.* **2001**, *114*, 5577.
(50) Kim, Y.; Ansari, S.; B.; Zwickel, B.; Meyer, H. *Rev. Sci. Instrum.* **2003**, *74*, 4805.
(51) Meyer, H. *J. Chem. Phys.* **1994**, *101*, 6686.
(52) Meyer, H. *J. Chem. Phys.* **1994**, *101*, 6697.
(53) Amiot, C.; Bacis, R.; Guelachvili, G. *Can. J. Phys* **1978**, *56*, 251.
(54) Miescher, E.; Huber, K. P. In *International Review of Science: Physical Chemistry, Series Two*; Buckingham, A. D., Ramsay, D. A., Eds.; Butterworths: London, 1973; p 37, Vol. 3.

JP811513J